

CHAPTER IV

RESULTS AND DISCUSSION

4.1 Amount of Precipitated Asphaltenes

The amount of asphaltenes that precipitated as a function of time from centrifugation experiments on Oil A at 60°C for 35 vol. % heptane, octane, nonane, and decane are shown in Figure 4.1.1. One can observe that different precipitants precipitate different amounts of asphaltenes due to different degrees of destabilization. Moreover, the times required for the amount of precipitated asphaltenes to reach a plateau value, the actual amount of precipitated asphaltenes at equilibrium, were approximately 70, 170, 200, and 270 hours for 35 vol. % heptane, octane, nonane, and decane respectively. This result suggests that the time required for the amount of precipitated asphaltenes to reach its plateau value increases with higher carbon number of precipitants. In addition, Figure 4.1.2 and 4.1.3 show the amount of precipitated asphaltenes from centrifugation experiments for Oil A at 60°C for 30 vol. % heptane and 40 vol. % decane respectively.

Although, the amount of precipitated asphaltenes as a function of time for Oil A at 60°C for 35 vol. % hexane was not shown due to fast asphaltenes precipitation, the amount of precipitated asphaltenes at equilibrium can be obtained. Figure 4.1.4 shows the amount of precipitated asphaltenes at equilibrium as a function of carbon number of precipitants. As can be seen, it seems to have an upward parabola trend as a function of carbon number, which is in a good agreement with previous work as shown in Figure 2.2.4 [Srikiratiwong, 2010].

In addition, all of the results for the quantity of asphaltenes precipitated as a function of time for Oil A diluted with heptane, octane, nonane, and decane at 60°C were used to calculate the collision efficiency, β , using the population balance model.

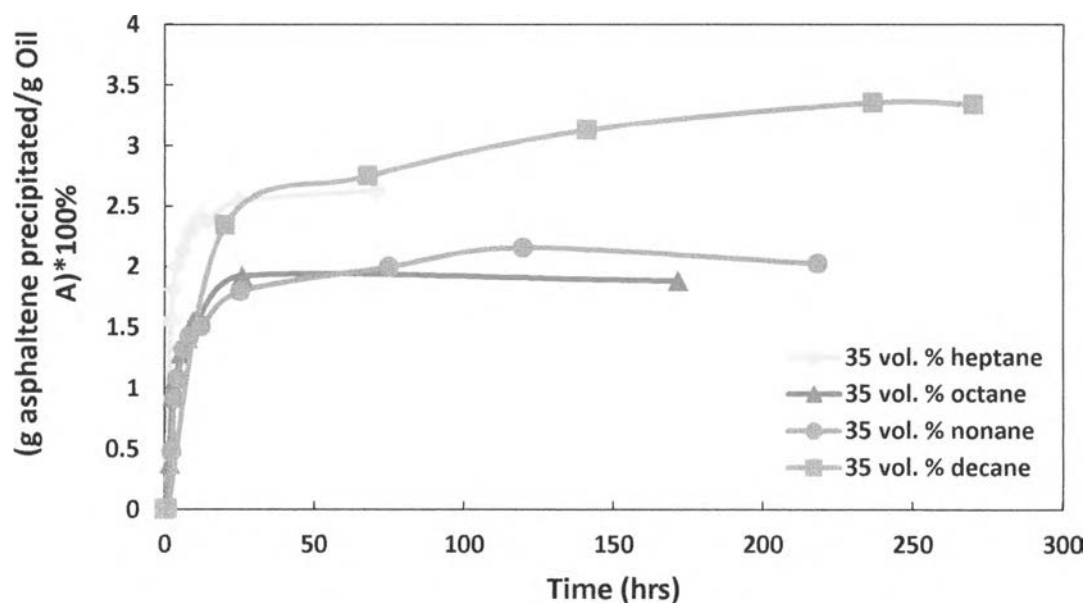


Figure 4.1.1 Amount of precipitated asphaltenes for Oil A at 60°C for 35 vol. % heptane, octane, nonane, and decane.

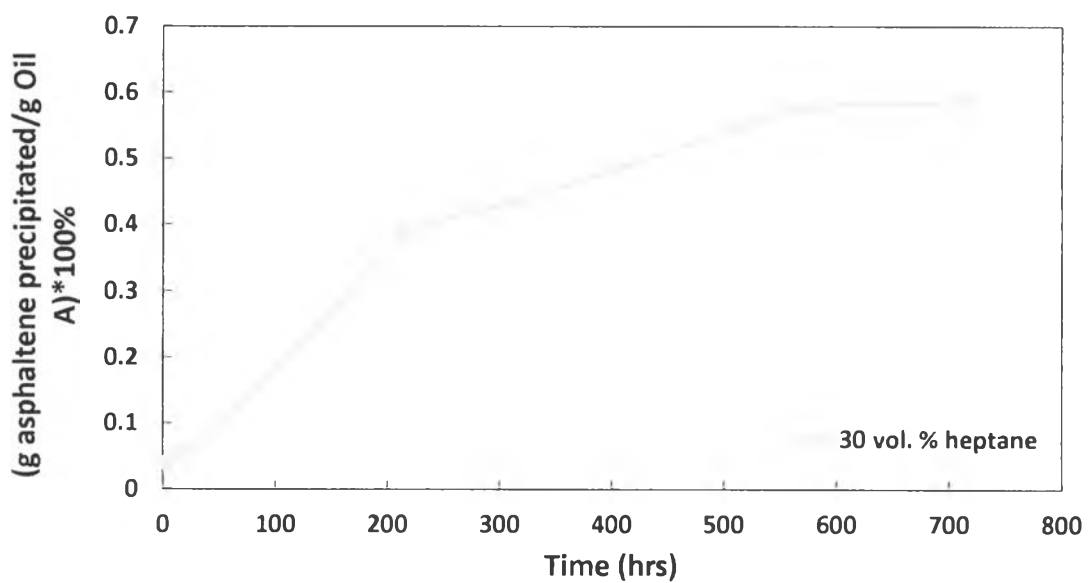


Figure 4.1.2 Amount of precipitated asphaltenes for Oil A at 60°C for 30 vol. % heptane.

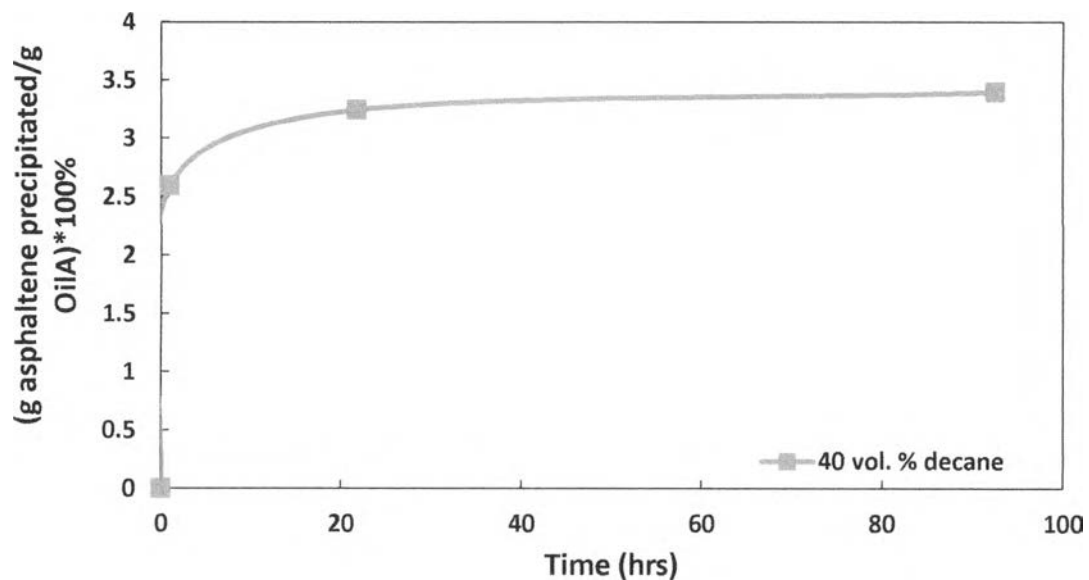


Figure 4.1.3 Amount of precipitated asphaltenes for Oil A at 60°C for 40 vol. % decane.

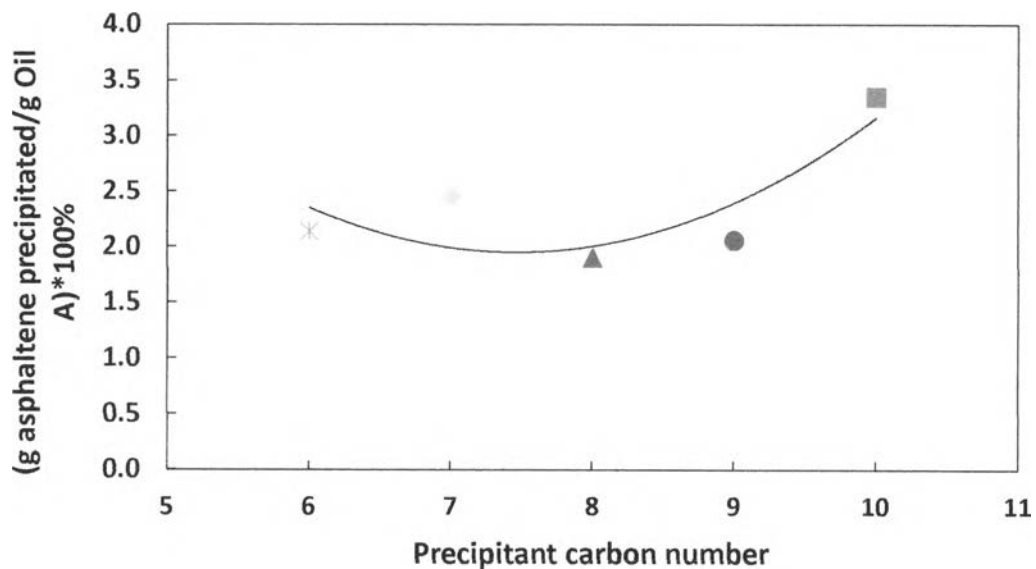


Figure 4.1.4 Amount of precipitated asphaltenes at equilibrium for 35 vol. % heptane, octane, nonane, and decane as a function of carbon number of precipitants at 60°C.

4.2 Collision Efficiency

Due to the complexity of the population balance model, MatLab was used to calculate the collision efficiency using the amount of precipitated asphaltenes as a function of time for Oil A at 60°C diluted with various precipitants and at various precipitant concentrations. It is to be noted that the code to calculate collision efficiency has already been written in MatLab from previous work [Maqbool *et al.*, 2011].

The best fit between the simulation and experimental results was defined as the one which minimized the Sum Square Error (SSE). SSE is defined as the discrepancy between the experimental data and the estimated results from the model was used. The lower value of SSE, the closer the simulation and the experimental results are. Figure 4.2.1 shows an example of the amount of asphaltene precipitated as a function of time at a minimum SSE between the simulated and experimental results for Oil A at 60°C and 35 vol. % heptane. It is important to note that all the data points were used to fit the population balance model in order to calculate the collision efficiency.

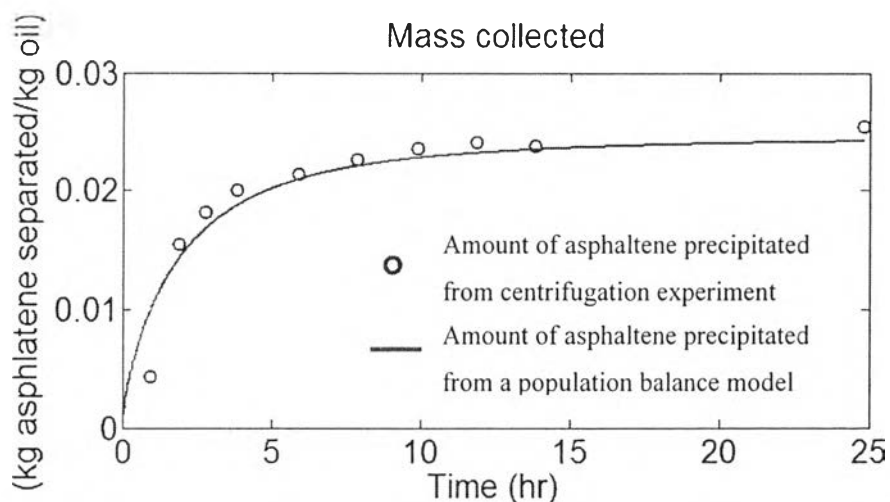


Figure 4.2.1 Amount of asphaltene precipitated as a function of time at minimum SSE between the simulated and experimental results for Oil A at 60°C and 35 vol. % heptane.

However, in order to estimate the accuracy of the calculated collision efficiency, the results of the amount of asphaltene precipitated as a function of time were divided into 2 portions to determine a maximum and minimum value of the collision efficiency. Figure 4.2.2 shows an example of amount of asphaltene precipitated as a function of time for Oil A at 60°C for 35 vol. % heptane that were divided into 2 portions. The destabilization of asphaltene is very rapid in the first set of data points so we assume 35% of the data is in this rapid destabilization region and to make all the data to be consistent, we employed this 35% threshold for all experimental data set. Thus, the first portion is the first 35% data of the amount of asphaltene precipitated and the second one is the rest of the data. The results in each portion were then used to calculate the collision efficiency using the population balance model in the same manner of using all experimental data, which was presented above. The amount of asphaltenes that precipitated as a function of time at minimum SSE between the simulated results using all, the first portion, and the second portion data and experimental results for Oil A at 60°C and 35 vol. % heptane are shown in Figure 4.2.3

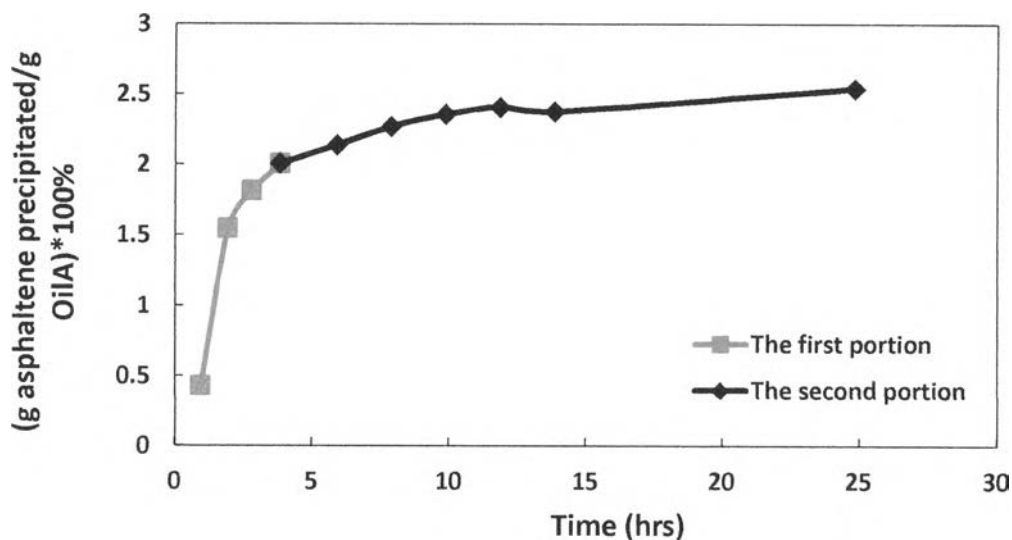


Figure 4.2.2 Amount of asphaltene precipitated as a function of time for Oil A at 60°C for 35 vol. % heptane.

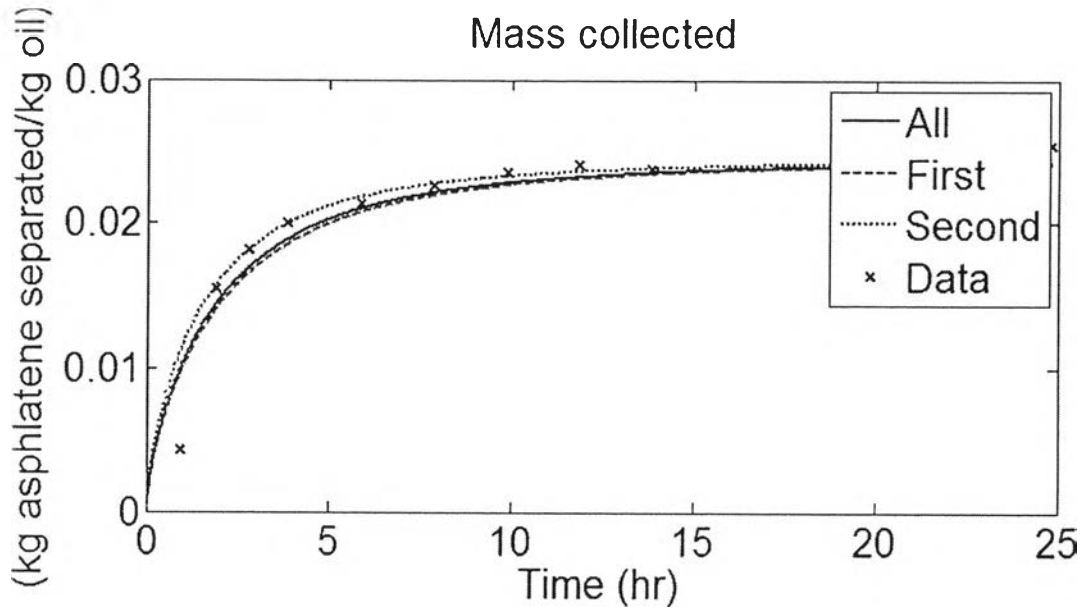


Figure 4.2.3 Amount of asphaltene precipitated as a function of time at minimum SSE between the simulated results using all, the first portion, and the second portion of the data and experimental results for Oil A at 60°C and 35 vol. % heptane.

From Haji Akbari Balou, N., 2013, collision efficiency is a function of the maximum potential barrier, U_{max} , and temperature and the maximum potential barrier, U_{max} is assumed to be inversely proportional to the difference between solubility parameter of asphaltene and solution squared, $(\delta_{asphaltene} - \delta_{solution})^2$, as shown in equation 4.2.1 and 4.2.2.

$$\beta = \exp\left(\frac{-U_{max}}{k_B T}\right) \quad (4.2.1)$$

$$U_{max} \propto \frac{1}{(\delta_{asphaltene} - \delta_{solution})^2} \quad (4.2.2)$$

where k_B is a Boltzman constant which is $1.3807 \times 10^{-23} \frac{m^2 kg}{s^2 K}$.

According to these two equations, and assuming that asphaltene solubility parameter is constant, the collision efficiency decreases with higher carbon number for a fixed volume fraction of precipitant. This is due to the fact that the solubility parameter of increases for higher carbon number precipitants.

Figure 4.2.4 shows the collision efficiency at minimum SSE with min-max error bar for Oil A at 60°C at different precipitants and precipitant concentrations. It can be observed that for a fixed volume fraction of precipitant, the collision efficiency decreases by approximately 25.4%, 39.9%, and 84.4% when the carbon number of precipitants increases from C7 to C8, C9, and C10 respectively indicating that the collision efficiency decreases with the higher carbon number of precipitants as expected. In addition, decreasing the precipitant concentration resulted in lower collision efficiency, which is consistent with previous work [Maqbool *et al.*, 2011].

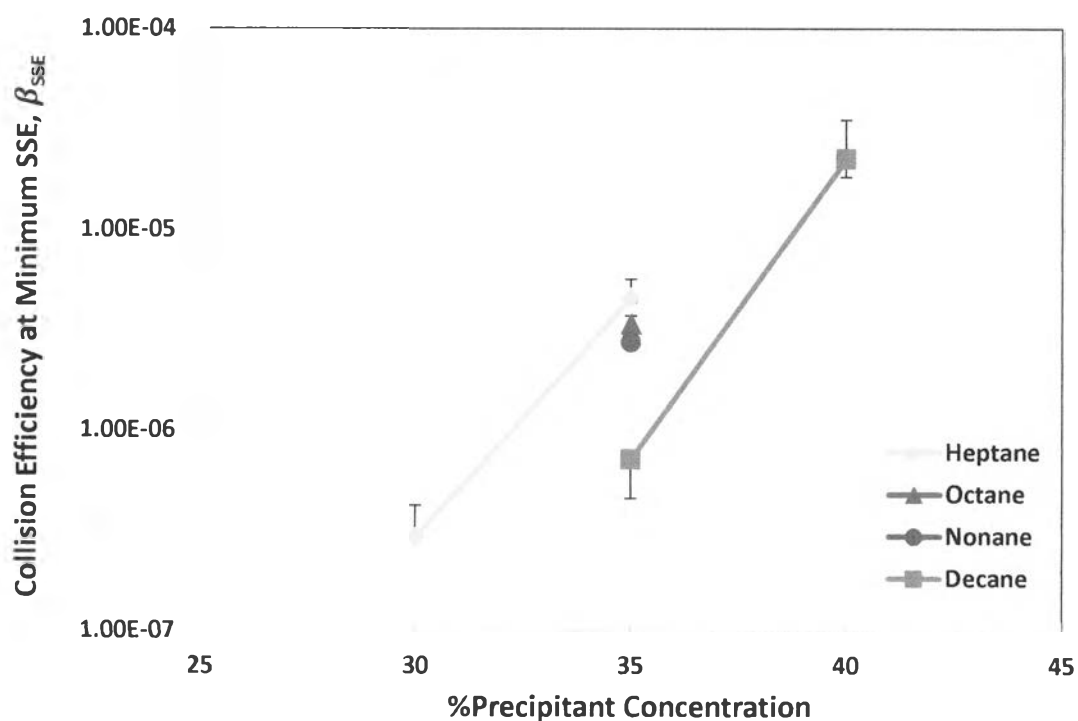


Figure 4.2.4 The collision efficiency at minimum SSE with min-max error bar for Oil A at 60°C for different precipitants and different precipitant concentrations.

4.3 A Correlation between Collision Efficiency and Solubility Parameter

From Haji AkibariBalou, N., 2013, the correlation between detection time, $t_{\text{detection}}$, and the difference between solubility parameter of asphaltene and solution squared, $(\delta_{\text{asphaltene}} - \delta_{\text{solution}})^2$, at 20°C using heptane as a precipitant was established as shown in equation 4.3.1.

$$\ln\left(\frac{t_{detection}\sqrt{C_0}}{\mu}\right) = \frac{3.31537 \times 10^9}{(\delta_{asphaltene} - \delta_{solution})^2} - 20.7119 \quad (4.3.1)$$

where $t_{detection}$ is the required time for asphaltene particles to reach 0.5 μm (s), μ is the viscosity of the mixture ($\text{Pa}\cdot\text{s}$), $\delta_{asphaltene}$ is asphaltene solubility parameter ($\text{Pa}^{0.5}$), $\delta_{solution}$ is solution (crude oil and precipitant) solubility parameter ($\text{Pa}^{0.5}$), and C_0 is number concentration of asphaltenes at $t=0$ ($\frac{\# \text{ monomer (asphaltene clusters)}}{\text{m}^3}$); $C_0 = 2.00738 \times 10^{25} \times b$ where b is volume of asphaltene (m^3) in 1 m^3 of solution.

By modifying this correlation, the correlation between detection time, $t_{detection}$, and the difference between solubility parameter of asphaltene and solution squared, $(\delta_{asphaltene} - \delta_{solution})^2$, at 60°C was obtained as shown in equation 4.3.2.

$$\ln\left(\frac{t_{detection}\sqrt{C_0}}{\mu}\right) = \frac{2.9171 \times 10^9}{(\delta_{asphaltene} - \delta_{solution})^2} - 14.5524 \quad (4.3.2)$$

where $C_0 = xy(1.4532 \times 10^{25})$; x is mass of asphaltene (kg) in 1 kg of crude oil and y is volume of crude oil (m^3) in 1 m^3 of solution.

Since detection time can be related to collision efficiency, the correlation between the collision efficiency and solubility parameter were investigated. First, the refractometer was used to measure the refractive index, n , of Oil A and precipitants at 60°C and a linear relationship between the refractive index and solubility parameter for paraffinic and aromatic hydrocarbons shown in equation 2.2.1 [Wang, J. X., and Buckley, J. S., 2001] was then used to determine the solubility parameter of Oil A and the precipitants. Table 4.3.1 shows refractive index and solubility parameter of Oil A and precipitants at 60°C .

Table 4.3.1 Refractive index and solubility parameter of Oil A and precipitants at 60°C

Chemicals	Refractive index, $n(nD_H)$	Solubility parameter, δ (MPa ^{0.5})
Oil A	1.5053	18.35
Hexane	1.3522	14.17
Heptane	1.3664	14.57
Octane	1.3777	14.89
Nonane	1.3861	15.13
Decane	1.3934	15.33

However, the relation between the RI and solubility parameter for paraffinic and aromatic hydrocarbons was established based on using ambient condition. Table 4.3.2 shows the comparison of solubility parameter between from Akbarzadeh's work in 2005 and the relation between the RI and solubility parameter for paraffinic and aromatic hydrocarbons at 60°C and the results indicates that this relation can be used to estimate solubility parameter at 60°C.

Table 4.3.2 Solubility parameter at 60°C from Akbarzadeh's work in 2005 and the relation between the RI and solubility parameter for paraffinic and aromatic hydrocarbons at 60°C.

Chemicals	Solubility parameter (MPa ^{0.5})			Using the relation	% error
	Akbarzadeh's work				
	Eq. (7)	Eq. (9)	Ref. (22)		
n-Hexane	13.87	14.07	14.20	14.17	1.59
n-Heptane	14.31	14.39	14.41	14.57	1.43

Using the volumetric average of solubility parameters of its components as shown in equation 4.3.3, the solution solubility parameter at 60°C can be estimated. The results shown in table 4.3.3 show the solution solubility parameter at 60°C for various volume % precipitants in Oil A.

$$\delta_{solution} = \sum_{i=1}^n x_i \delta_i \quad (4.3.3)$$

where $\delta_{solution}$ is solution solubility parameter (MPa^{0.5}), x_i is volume fraction of each component, δ_i is solubility parameter of each component (MPa^{0.5}), and n is number of component.

Table 4.3.3 Solution solubility parameter at 60°C for various volume % precipitants in Oil A

Volume % precipitant in Oil A	Solution solubility parameter (MPa ^{0.5})
30 vol. % heptane	17.22
35 vol. % heptane	17.03
35 vol. % octane	17.14
35 vol. % nonane	17.22
35 vol. % decane	17.29
40 vol. % decane	17.14

Moreover, onset experiments for Oil A at 60 °C for 35 vol. % heptane, octane, nonane, and decane were performed to obtain the detection time, and the results are shown in Figure 4.3.1. From the detection time and solution solubility parameter results, the asphaltene solubility parameter at 60°C for heptane, octane, nonane, and decane can be calculated from equation 4.3.2 and the result is shown in Figure 4.3.2. It can be observed that the detection time and solution solubility parameter increase with higher carbon number of precipitants, suggesting that asphaltenes at higher carbon number of precipitants tend to have smaller tendency to

precipitate resulting in higher asphaltene solubility parameter. In this investigation, the asphaltene solubility parameter was assumed to be a constant as a function of the precipitant concentration but was varied for each precipitant type.

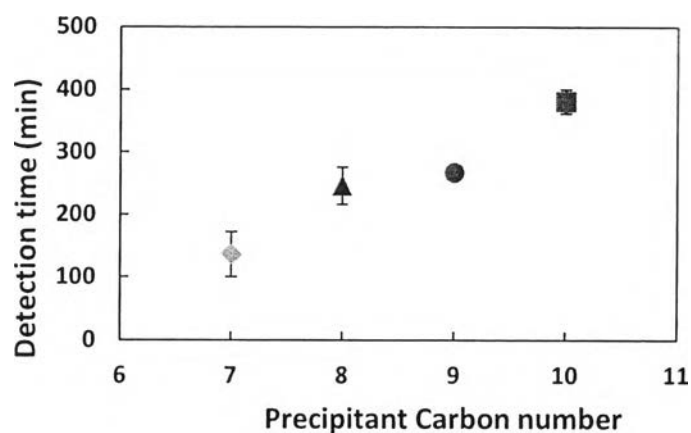


Figure 4.3.1 Detection time for Oil A at 60°C for 35 vol. % heptane, octane, nonane, and decane.

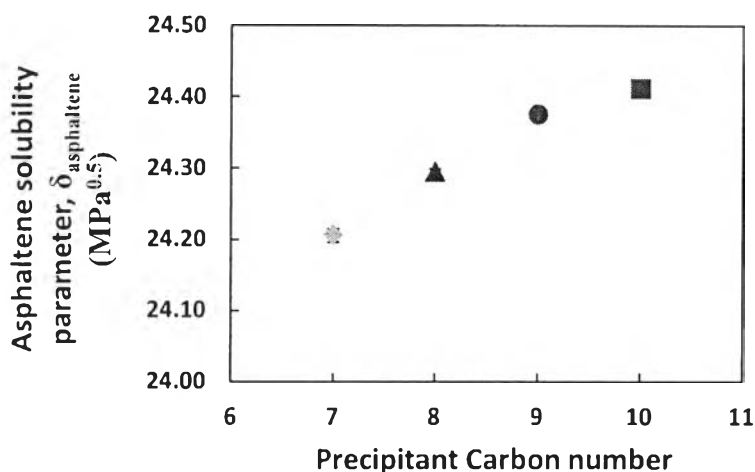


Figure 4.3.2 Asphaltene solubility parameter for Oil A at 60°C for heptane, octane, nonane, and decane.

By obtaining the collision efficiency, asphaltene solubility parameter, and solution solubility parameter, the correlation between the collision efficiency and solubility parameter for Oil A at 60 °C was established as shown in Figure 4.3.3. This correlation can be used to estimate the collision efficiency for Oil A at 60 °C for other precipitants and precipitant concentrations. It can also be utilized further in actual oil field conditions where the precipitant is methane and the collision

efficiency of the asphaltenes can be estimated and consequently the aggregation rate of asphaltene may be achieved.

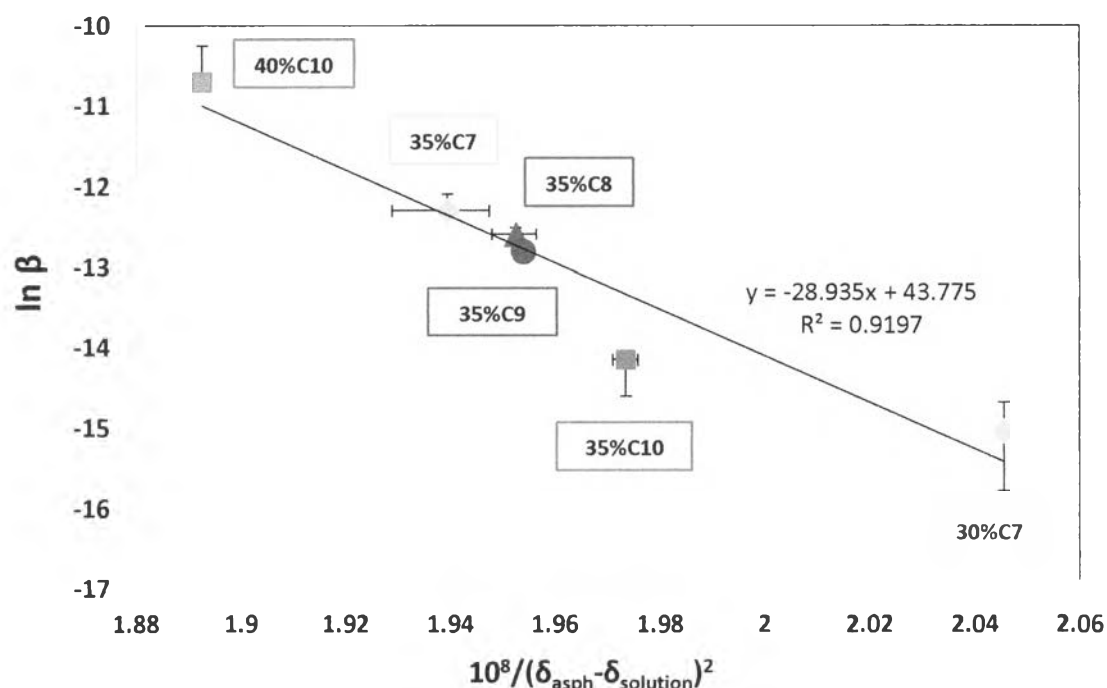


Figure 4.3.3 The correlation between collision efficiency and solubility parameter for Oil A at 60°C.

4.4 Asphaltene Deposition

Figure 4.4.1 shows the results of $(\Delta P - \Delta P_0)$ vs. time for Oil A at 60°C and at a total flow rate of 5 mL/h for 35 and 30 vol. % heptane using the capillary deposition apparatus. It can be observed that at 35 vol. % heptane, the deposition was detected sooner than at 30 vol. % heptane because higher precipitant concentrations have more destabilized asphaltenes, which results in a greater increase in the pressure drop across the capillary. This observation is in a good agreement with previous work [Hoepfner *et al.*, 2013].

Moreover, the pressure drop trajectory plots in Figure 4.4.1 were compared with previous results [Hoepfner *et al.*, 2013] at the same operating conditions as shown in Figure 4.4.2. Since all of the experimental conditions between the current results and the previous results are the same, both pressure drop trajectory should

superimpose with each other. However, it was found that the slopes between the pressure drop and time results of the current results are lower than that of the previous results.

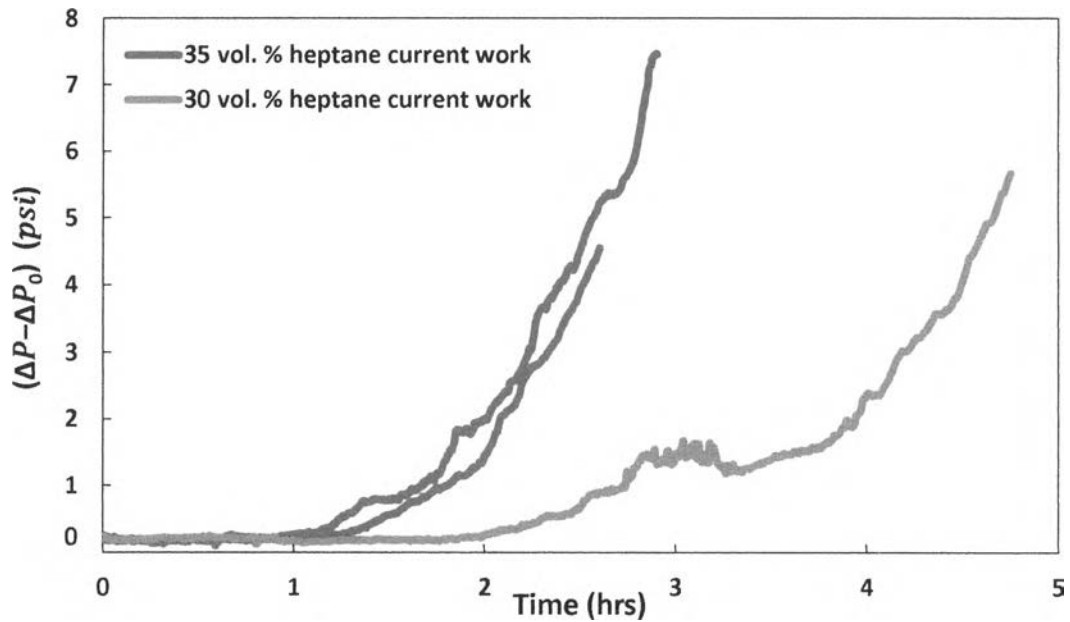


Figure 4.4.1 Pressure drop trajectory for Oil A at 60°C for 35 and 30 vol. % heptane.

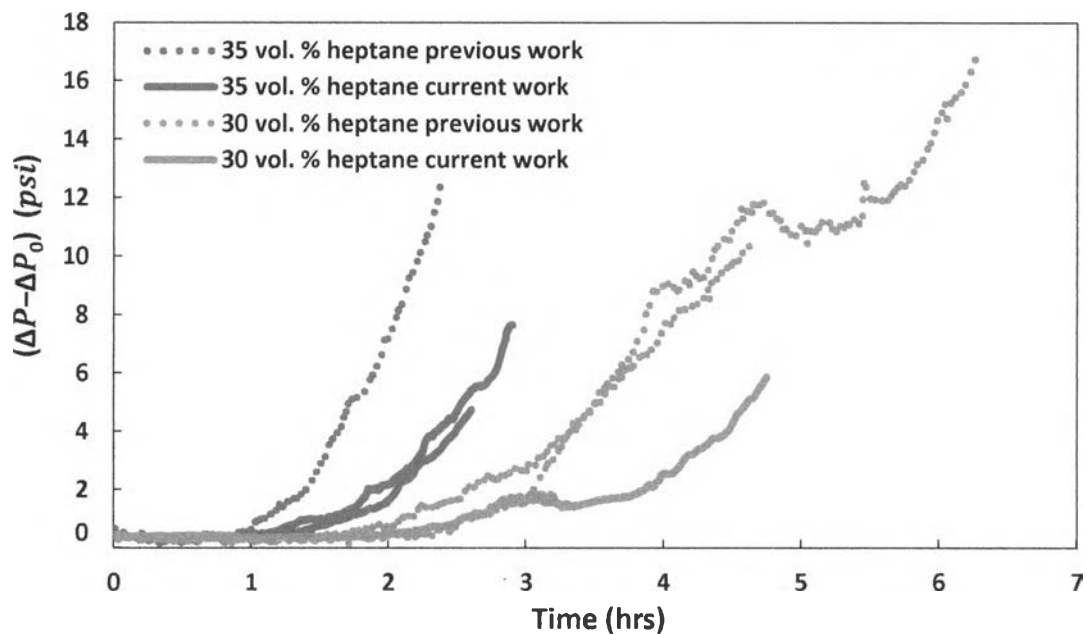


Figure 4.4.2 Pressure drop trajectory of the previous and current results for Oil A at 60°C for 35 and 30 vol. % heptane.

To investigate this deviation, the capillary inner diameters were measured, as discussed in the experimental procedure. Nominally, the inner diameters of the capillaries in all the experiments were 0.01 inch; however, small deviations could occur. Figure 4.4.3 shows the measured capillary inner diameters, and it was observed that the capillary diameters from previous results are smaller than that from current results. The average capillary diameter from the current results is 0.0105 inches and the average capillary diameter from previous results is 0.0077 inches. Therefore, it can be concluded that the shift of the slope in the current results is due to bigger inner diameters of the capillary tubes. Thus, to compare the pressure drop trajectory at different runs, radius of capillary (r) was used to normalize the pressure drop data.

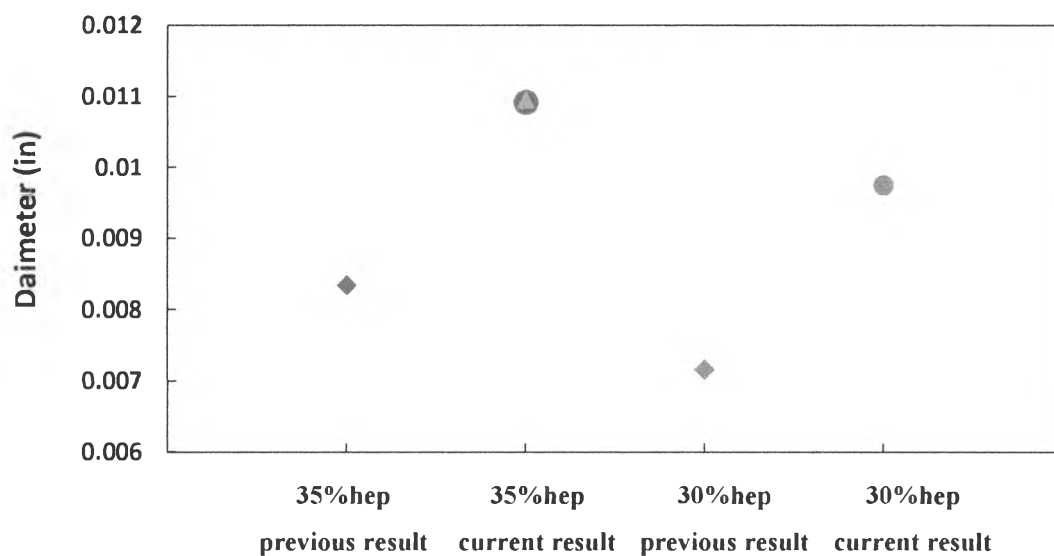


Figure 4.4.3 Capillary diameters of 35 and 30 vol. % heptane of previous results and current results.

Figure 4.4.4 shows the pressure drop trajectory for Oil A at 60°C for 35 and 30 vol. % heptane after normalization by the inner radius of the capillaries (r). It revealed that the results from previous work and the current work superimpose with each other, indicating that after the radius of capillary (r) was taken into account, the results were reproducible and consistent.

In addition, viscosity of mixture (μ), mass fraction of insoluble asphaltenes precipitated from crude oil (F), and the volume fraction of crude oil (Φ_{oil}) were also used to normalize the data as shown in Figure 4.4.5 since various precipitants and precipitant concentrations were investigated in this study. This normalization was done in the same manner as in the work of Hoepfner *et al.*, 2013.

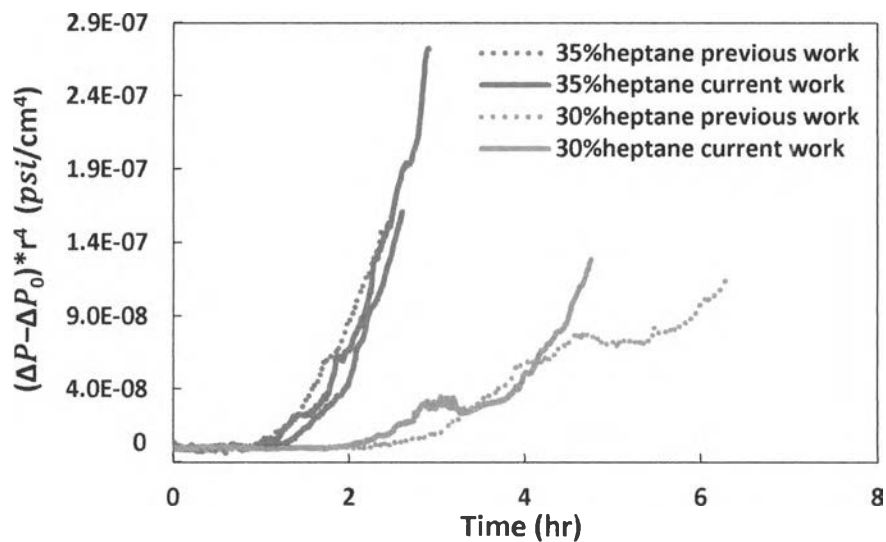


Figure 4.4.4 The pressure drop trajectory for Oil A at 60°C for 35 and 30 vol. % heptane normalized by using radius of capillary.

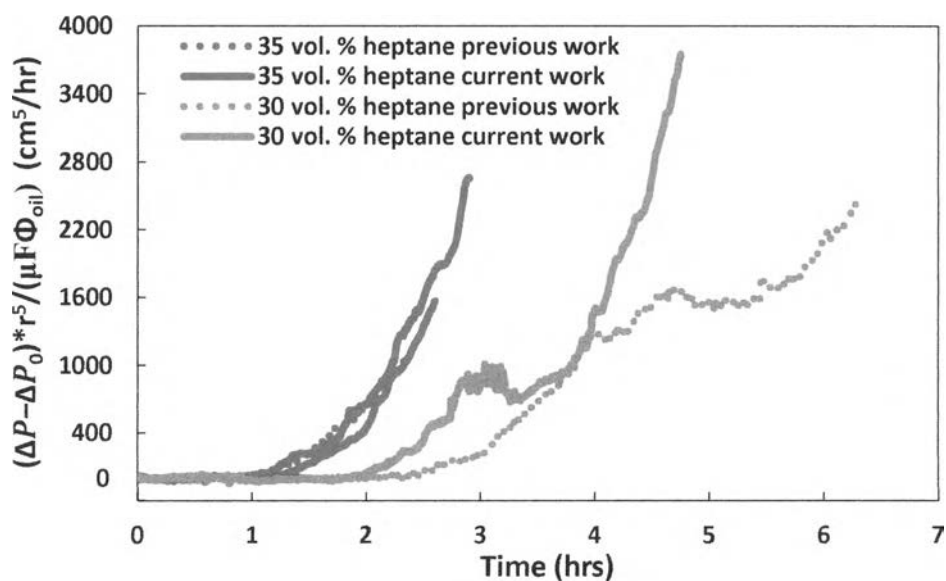


Figure 4.4.5 The normalized pressure drop trajectory for Oil A at 60°C for 35 and 30 vol. % heptane.

First, decane was used as a precipitant to investigate asphaltene deposition because the biggest difference in collision efficiency was observed between decane and heptane as shown in Figure 4.2.4 for 35 vol. % of precipitants. However, in Figure 4.4.6, the pressure drop trajectories for Oil A at 60°C for 35 vol. % decane shows inconsistent results for four, as observed by differences and fluctuations in the pressure drop. One of the possible explanations for the inconsistency is that Oil A and decane were not homogeneously mixed when they entered the capillary test section. In order to investigate this, SEM images of the deposit at the capillary inlet of 35 vol. % decane in Oil A were taken as shown in Figure 4.4.7. It can be observed that the deposit did not form around the entire capillary inlet, instead it formed a bridge-shaped deposit (image b). One of the two holes was either oil-rich or decane-rich and the deposit was forming rapidly at the junction of those two holes indicating poor mixing in the system. Thus, it can be concluded that due to mixing issue, decane cannot be used to investigate asphaltene deposition without modifying the apparatus to improve the mixing. However, if the apparatus were modified, the heptane results would not be able to compare with the previous work [Hoepfner *et al.*, 2013] so other precipitants that have lower viscosity were used to investigate asphaltene deposition since the lower viscosity increases quality of mixing.

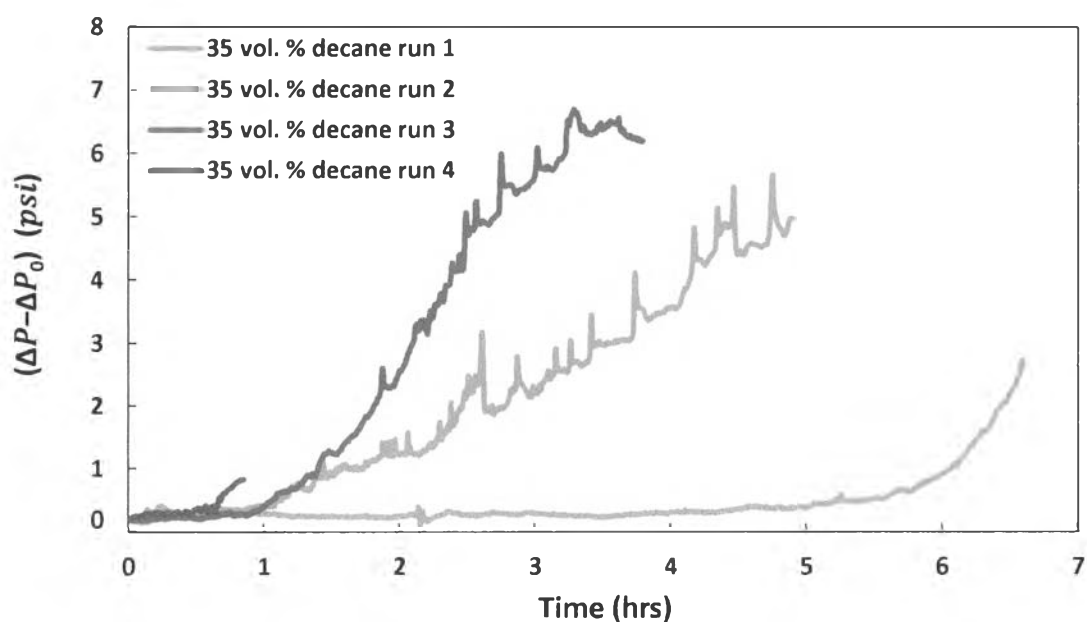


Figure 4.4.6 The pressure drop trajectory for Oil A at 60°C for 35 vol. % decane.

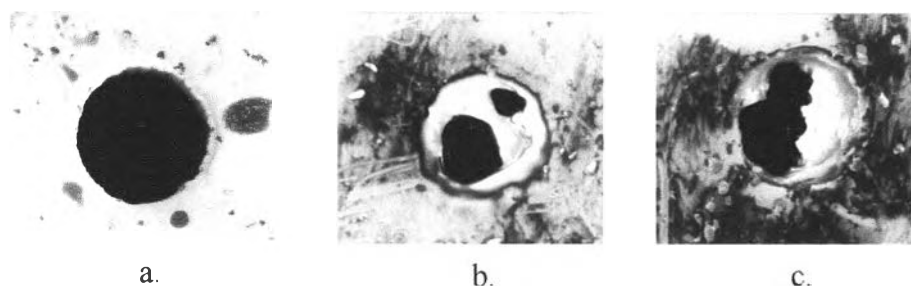


Figure 4.4.7 SEM images of the deposit at capillary inlet of 35 vol. % decane in Oil A. Image a. is an unused capillary inlet and images b. and c. are used capillary inlet.

Octane and hexane were used as precipitants and the results shown in Figures 4.4.8 and 4.4.9 shows the pressure drop trajectory normalized by r , μ , F , and Φ_{oil} , the capillary diameter measurement results are shown in table 4.1, for Oil A at 60°C for 35 vol. % octane and hexane, respectively. It can be seen that the normalized pressure drop trajectory for 35 vol. % octane and hexane was consistent and reproducible compared to the normalized pressure drop trajectory for 35 vol. % decane. The mixing quality was also investigated using SEM and the SEM images of the deposit at the capillary inlet of 35 vol. % octane and hexane in Oil A were taken and shown in Figure 4.4.10. From the SEM images, the deposit formed around the entire capillary inlet, which indicates good mixing and is in a good agreement with the pressure drop results.

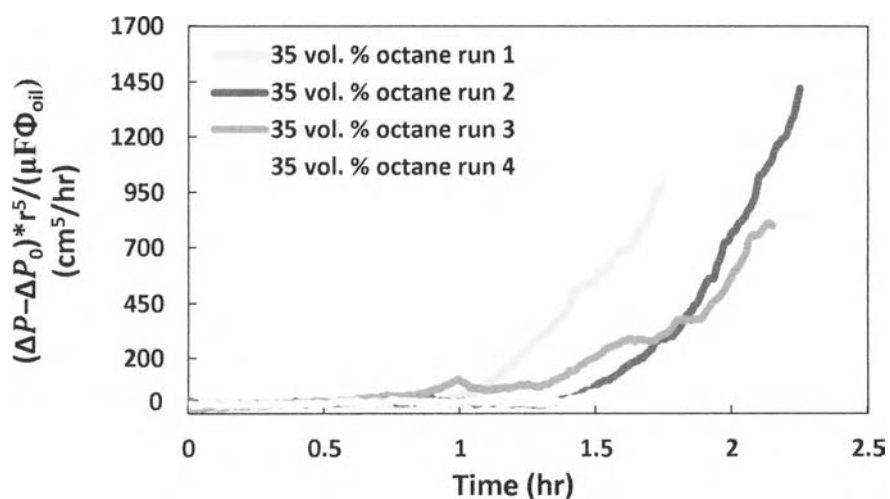


Figure 4.4.8 The normalized pressure drop trajectory for Oil A at 60°C for 35 vol. % octane.

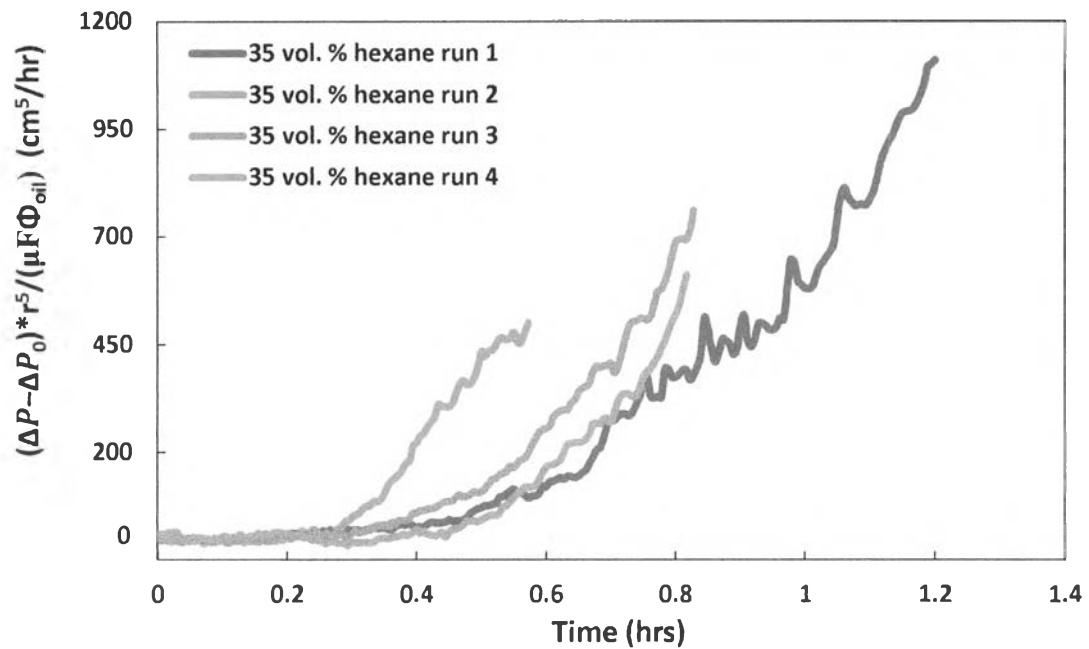


Figure 4.4.9 The normalized pressure drop trajectory for Oil A at 60°C for 35 vol. % hexane.

Table 4.4.1 Capillary Diameters

	Run	Average Capillary diameter (in)	Average Capillary diameter (cm)
35 vol. % octane	1	0.01050	0.02668
	2	0.01055	0.02680
	3	0.01005	0.02554
	4	0.01011	0.02568
35 vol. % hexane	1	0.01001	0.02543
	2	0.01052	0.02671
	3	0.01055	0.02679
	4	0.01007	0.02558

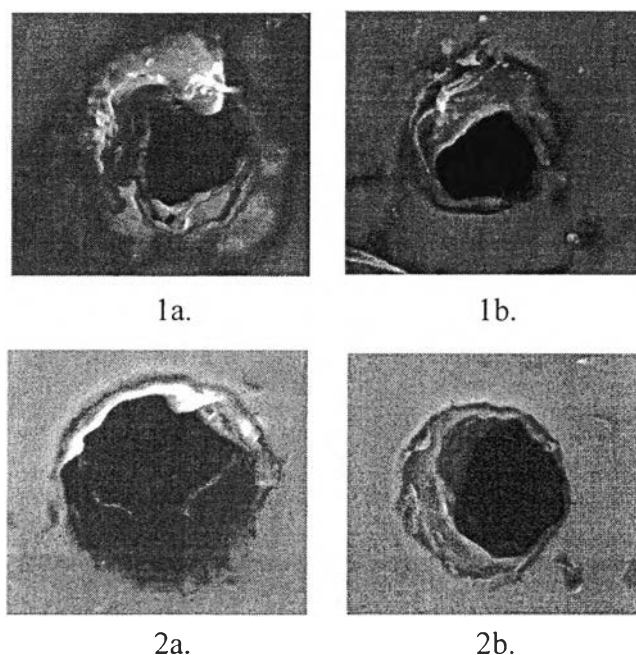


Figure 4.4.10 SEM images of the deposition capillary inlet of 35 vol. % octane (1a. and 1b.) and hexane (2a. and 2b.) in Oil A.

In order to compare the normalized pressure drop trajectory for Oil A at 60°C for 35 vol. % heptane, octane, and hexane and 30 vol. % heptane, they were plotted together in Figure 4.4.11. It can be seen that the induction time, the time required until the pressure drop can be detected, increases from 0.25 hours for hexane to 0.94 hours for heptane and to 1.05 hours for octane at 35 vol. % of precipitant, suggesting that higher carbon number of precipitants have weaker destabilized asphaltenes and is in agreement with the onset experiment results in Figure 4.3.1.

Although, one of the 35 vol. % octane runs appears to deviate from the other runs, it could be due to the sensitivity of the apparatus.

After removing the induction time and averaging all the results, it was found that the slopes of all pressure drop trajectory are approximately the same after pressure drop was normalized using radius of capillary tube (r), viscosity of mixture (μ), mass fraction of insoluble asphaltenes precipitated from crude oil (F), and the volume fraction of crude oil (ϕ_{oil}). It indicates that the differences in collision efficiency for different precipitants and precipitant concentrations as shown in Figure 4.4.12, did not appear to influence the normalized deposition behavior.

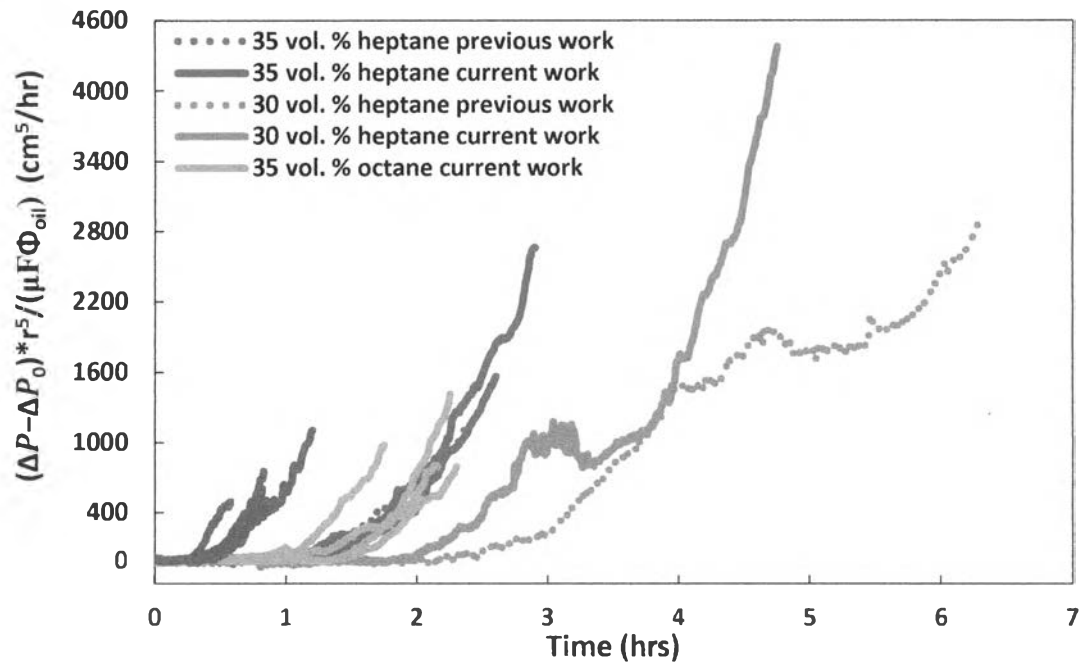


Figure 4.4.11 The normalized pressure drop trajectory for Oil A at 60°C for various precipitants and precipitant concentrations.

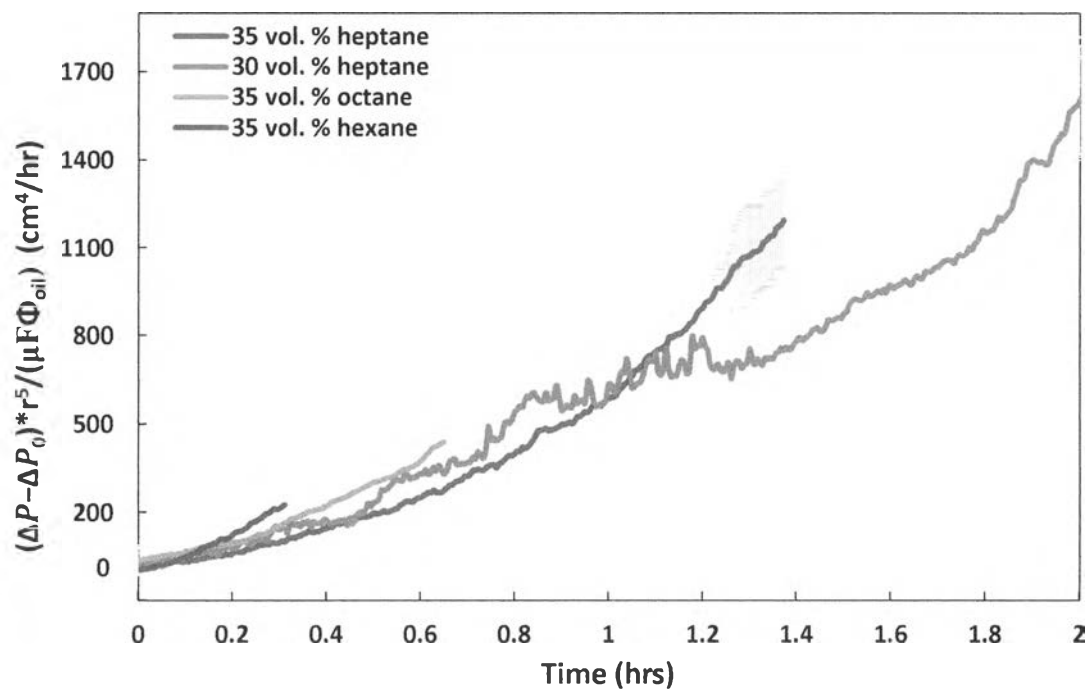


Figure 4.4.12 The average of normalized pressure drop trajectory for Oil A at 60°C for various precipitants and precipitant concentrations without the induction time.